Theor Chem Acc (1998) 100:147–153
DOI 10.1007/s002149800m56

Theoretical
Chemistry Accounts

Regular article

Periodic orbits and vibrational wave functions for DCP: nonlinear resonances in isotopically substituted molecules*

Stavros C. Farantos[1], Christian Beck[2], Reinhard Schinke[2]

[1]Institute of Electronic Structure and Laser Foundation for Research and Technology, Hellas, and Department of Chemistry University of Crete, 711 10 Iraklion, Crete, Greece
[2]Max-Planck-Institut für Strömungsforschung, D-37073 Göttingen, Germany

Received: 24 June 1998 / Accepted: 10 August 1998 / Published online: 9 October 1998

Abstract. We investigate, by means of classical and quantum mechanics, how isotopic substitution (H/D) affects the vibrational dynamics of HCP. The analysis of periodic orbits, including the location of the principal families as well as saddle node bifurcations, reveals a totally different picture for the phase-space resonance structure for HCP and DCP. While HCP is characterized by a 1:2 resonance between the CP stretch and the bending mode, DCP shows a 1:2 resonance between the two stretching degrees of freedom. Saddle node bifurcations, which are associated with large-amplitude motion of H/D moving from the C- to the P-end, appear at considerably higher energies in DCP than in HCP. These results are in accord with exact quantum mechanical calculations of the vibrational levels.

Key words: Vibrational spectroscopy –
Highly excited states – Periodic orbits – Bifurcations

1 Introduction

Isotopic substitution is a well-established method in molecular spectroscopy for assigning vibrational levels and, in general, for investigating the multi-dimensional motion on potential energy surfaces (PES). The replacement of a particular atom in a molecule by its isotope affects only the kinetic part of the Hamiltonian but leaves the PES unchanged. As a consequence, this modifies the fundamental vibrational frequencies and thus changes the zero-point energy of the system. The resulting effects are normally largest when hydrogen is replaced by deuterium.

At low energies, isotopic substitution is expected to cause only a shift of the vibrational levels but no significant changes in the overall spectral patterns. However, the situation might be quite different if the spectrum is governed by an anharmonic resonance (i.e., the near degeneracy of two or more lower vibrational states); such a resonance can be dramatically changed by isotopic substitution. Examples are HCO/DCO [1, 2] and HNO/DNO [3]. Moreover, isotope substitution might cause substantial changes in the level spectrum at higher vibrational excitations in those cases where the kinetic part of the Hamiltonian leads to strong couplings among several degrees of freedom.

A molecule which has been found to show a pronounced anharmonic resonance effect all the way from the bottom of the potential well to high excitation energies and, in addition, peculiar nonlinear dynamics effects at high energies is phosphaethyne (HCP). In two previous publications [4, 5] we have presented a detailed classical and quantum mechanical study of its vibrational motion up to an energy range of about 3 eV above the minimum of the potential.

HCP has been of interest to spectroscopists for several years. Equilibrium geometries and spectroscopic constants of the ground and the first excited electronic states have been determined by electronic, vibrational, and rotational spectra [6–10]. Our interest in this molecule was particularly stimulated by the studies of Field and coworkers [11, 12], who accessed high-lying bending vibrational states by exploiting the $\tilde{A} - \tilde{X}$ and $\tilde{C} - \tilde{X}$ transition bands. Both dispersed fluorescence and stimulated emission pumping (SEP) experiments were carried out.

Our previous calculations for HCP as well as experimental results showed quite regular behavior up to relatively high energies; for example, the majority of states can be uniquely assigned by three quantum numbers. The energy spectrum is governed, from the lowest excited states up to very high excitation energies, by a 1:2 anharmonic resonance between the HCP bending and the CP stretching mode (two quanta of the bend are almost equal to one quantum of the CP stretch) [13, 14]. This leads to a pronounced clustering of the states in terms of polyads [15, 16]. Families of periodic orbits (POs) [17–20] and particularly the construction of

* Dedicated to Prof. Dr. Wilfried Meyer on the occasion of his 60th birthday

Correspondence to: R. Schinke

a continuation/bifurcation diagram were used to predict and assign families of wave functions localized in particular regions of configuration space [4, 5] .

In our classical/quantum study two observations came as a surprise. First, up to an energy of about 2.2 eV above the minimum all wave functions as well as POs are confined to a very small angular range around the linear geometry – despite the fact that energetically a much wider angular range would be accessible. Second, states and POs which slowly begin to explore the isomerization path from H–CP to CP–H suddenly occur at a relatively high threshold energy. These states were termed saddle node (SN) states because they are associated with SN bifurcations of POs. It was demonstrated that these SN states possibly explain some of the peculiarities found in the measured fine structure constants.

In the previous study of HCP we showed that the 1:2 resonance is sensitive to the mass of the light atom. The purpose of the present article is to explore the resonance structure of the phase space in DCP and to see how the vibrational level pattern changes with respect to HCP.

2 Calculational methods

The PES used for the present calculations is the same as that employed for HCP and is described in Ref. [5]. This PES provides a realistic description of the internal vibrational dynamics; however, it is not sufficiently accurate to allow direct comparison with experimental data. A new global ab initio PES is presently under construction and will be published at a later date.

The classical mechanics and the quantum mechanical calculations are performed in the Jacobi coordinates R, the distance from D to the center-of-mass of CP, r, the CP separation, and γ, the angle between the vectors $\mathbf{R}$ and $\mathbf{r}$ (with $\gamma = 0$ for linear DCP). In what follows all energies are quoted with respect to the minimum of $D + CP(r_e)$. In this normalization the energy at the equilibrium is $-5.2361\,\text{eV}$ ($R = 4.1572a_0$, $r = 2.9444a_0$, $\gamma = 0$). The energy and the coordinates of the CP–D saddle point are $-1.8935\,\text{eV}$, $R = 3.5634a_0$, $r = 3.0904a_0$, and $\gamma = 180°$, respectively. The total angular momentum is $J = 0$ in both the classical and quantum calculations.

Periodic classical orbits are located by multiple shooting algorithms and by damped and quasi-Newton iterative methods [21]. For a system with three degrees of freedom there are three families of POs which emanate from the stable equilibrium point of the PES. These families are called principals and correspond to the three normal vibrational modes. By following the evolution of the principal families with total energy, one can locate new families of POs, which bifurcate from the parent ones; they start either with the same periods as the original POs or multiples of them. New POs may also appear via SN bifurcations. These bifurcations emanate suddenly at particular excitation energies, usually as pairs of POs with one of them being stable and the other being unstable. A PO is stable when trajectories started close to it stay in its vicinity for all times. On the other hand, a PO is unstable when trajectories that are launched close to it depart exponentially, i.e., the "distance" between the two trajectories in phase space grows exponentially with time. Instability may not grow simultaneously for all degrees of freedom but only for some of them. Therefore, POs are described as single unstable, double unstable, etc [20].

We have also performed quantum mechanical variational calculations for determining the vibrational energies as well as the corresponding wave functions. The Hamiltonian is represented in a highly contracted/truncated 3D basis as described in detail in Ref. [22]. The variational program requires two parameters: the energy E_{cut} up to which all internally contracted basis functions are included and the maximum distance of the dissociation coordinate, $R_{\max}$. All other parameters are chosen automatically. In the calculations we used $E_{\text{cut}} = -1.0\,\text{eV}$ and $R_{\max} = 6.22a_0$. In the present work we analyzed only the 200 lowest quantum states or so with energies up to about $-3.4\,\text{eV}$; for this restricted range of energies the two parameters guarantee a convergence of at least 0.1 meV.

3 Results and discussion

3.1 Vibrational states of HCP

In this section we briefly summarize – for comparison with the results for DCP – the main conclusions of our study of HCP.

The spectrum is governed by a 1:2 resonance between CP stretching and HCP bending motion leading to substantial mixing of (zero-order) local-mode states [13, 14]. This resonance appears from almost the zero-point level and results in a spectrum which consists of clearly defined polyads. The normal-mode wave functions are highly regular, even at energies where anharmonic couplings due to the potential are prominent. In terms of POs, the anharmonic resonance is the result of a bifurcation of the $[r]$-stretching (CP vibration) family of POs, which actually happens below the quantum mechanical zero-point energy. The original period is doubled in this bifurcation. The POs belonging to the new, i.e., the bifurcated branch, termed $[r1A]$, and the POs constituting the bending family, $[B]$, are confined to the H–CP hemisphere, i.e., the (Jacobi) angle γ remains smaller than about 40°, even if the energy is sufficiently high to allow the isomerization path to CP–H to be followed. The close correspondence of the POs and the quantum wave functions guarantees the same qualitative behavior for the quantum mechanical eigenfunctions.

States which do follow, with increasing energy, the isomerization path all the way to the CP–H side, suddenly come into existence at a relatively high energy.

Table 1. Energies E, periods T, and initial conditions for selected periodic orbits (POs)

PO	E/eV	T^{a}	R^{b}	r	γ	p_R	p_r	p_γ
$[R]$	−2.526612	1.665	2.1079393	1.6653515		2.2761880	−2.2456483	
$[R1A]$	−2.5244452	2.867	2.2673398	1.7232877		2.6327799	2.2181170	
$[r]$	−2.2627475	3.215	2.3423666	1.6652200		1.5003978	5.9658228	
$[B]$	−2.6217276	9.680	1.7596965	1.6253361	0.8754786	−0.6579276	−1.2351993	1.1410343
$[SN1A]$	−1.5284771	15.265	2.7593397	1.5670530	0.0724694	−0.5869885	0.6108876	4.4889123
$[SN1B]$	−1.5383796	12.600	2.5931984	1.8447965	−0.07571909	0.41063180	0.4169811	5.6372880

[a] One time unit corresponds to 10.18 fs
[b] Distances in Å, angle in radians

They replace the normal-mode like $[r1A]$ stretching states at the bottom of the polyad. The new class of bending states, which are called SN states, is consistent with the appearance of POs from SN bifurcations. The SN POs describe the isomerizing states remarkably well, i.e., the backbones of the quantal wave functions closely follow the $[SN]$ POs. The first SN bifurcation was located at -3.1526 eV and more were found at higher energies.

Although direct comparison with experimental data is not possible at present because of the limited accuracy of the PES used, our calculations qualitatively explained several observations such as (1) the abrupt onset of perturbations found in the experimental SEP spectra, (2) the existence of states with two classes of rotational constants, and (3) the reality of states with unusually large anharmonicities.

3.2 Vibrational states of DCP

3.2.1 The classical view

The organization of the classical phase space of DCP in a hierarchical way is revealed by the continuation/bifurcation diagram of POs depicted in Fig. 1. One particular 'initial' coordinate, R in the present case, of each PO as a function of E is shown in Fig. 1a (for more details see Ref. [5]); each point on a continuation/bifurcation line actually corresponds to one particular PO. The associated periods as a function of energy are plotted in Fig. 1b. The equivalent pictures for HCP are given in Ref. [5]. POs have been located for the energy interval from the bottom of the potential well, -5.236 eV, up to -1 eV . The continuation of a family of POs is manifested by a continuous smooth line. Following a similar notation as was used for HCP, we denote the principal families by $[B]$ for the bending mode, $[R]$ for the R-stretching mode, and $[r]$ for the r-stretching mode. The $[R1A]$ family is a bifurcation of the $[R]$ principal family, and $[SN1A]$ and $[SN1B]$ are the two branches of a SN bifurcation. Notice, that in the SN bifurcation the period of one branch strongly increases with energy while in the other branch it slightly decreases.

Representative POs, for relatively high energies, are shown in Figs. 2 and 3 together with contours of the PES. The stretching POs have no extension in the bending mode and they always remain in the $(r, R, \gamma = 0)$ plane. The POs in Fig. 2 correspond to the energies -2.5266, -2.5244 and -2.2627 eV for the $[R]$, $[R1A]$, and $[r]$-type POs, respectively. Their periods are 16.9, 29.2, and 32.7 fs. Note that the $[R]$ and $[r]$ POs are almost perpendicular to each other. The $[R1A]$ PO is a mixture of R and r motion. Figure 3 shows two POs of the bending type with energies of -2.6217 and -1.6195 eV, and one $[SN1]$-type PO with energy -1.5285 eV. Their periods are 98.6, 110.8, and 155.4 fs, respectively. Both projections in the (R, γ) and in the (r, γ) plane are presented. Notice the relatively small extension of the $[B]$-type POs in the angle coordinate, less than 60°, in spite of the very high energy above the bottom of the well;

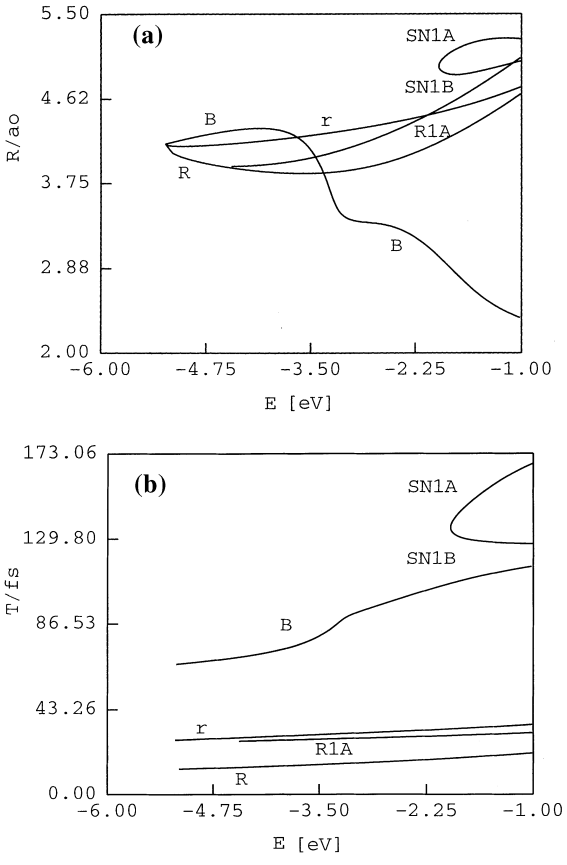

Fig. 1. a Continuation/bifurcation diagram showing the variation of the initial R stretching coordinate as function of energy. For further details see the text. **b** The periods (in fs) of the $[B]$-, $[R]$-, $[R1A]$-, $[r]$- and $[SN]$-type periodic orbits (POs) as functions of energy

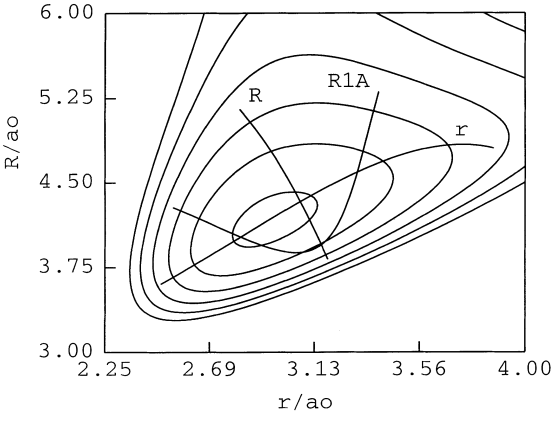

Fig. 2. Contour plot of the HCP potential energy surface as a function of r and R for $\gamma = 0$. Energy normalization is such that $H + CP(r_e)$ corresponds to $E = 0$. The highest contour is for $E = 0$ and the spacing is $\Delta E = 1$ eV. Also shown are projections of selected classical POs: $[r]$, $E = -2.262747$ eV; $[R]$, $E = -2.526612$ eV; $[R1A]$, $E = -2.524445$ eV

although the energy difference between the two orbits is about 1 eV, they cover the same angular range. Generally, we find significant variation in the shape of the $[B]$ orbits above an energy of -3.4 eV.

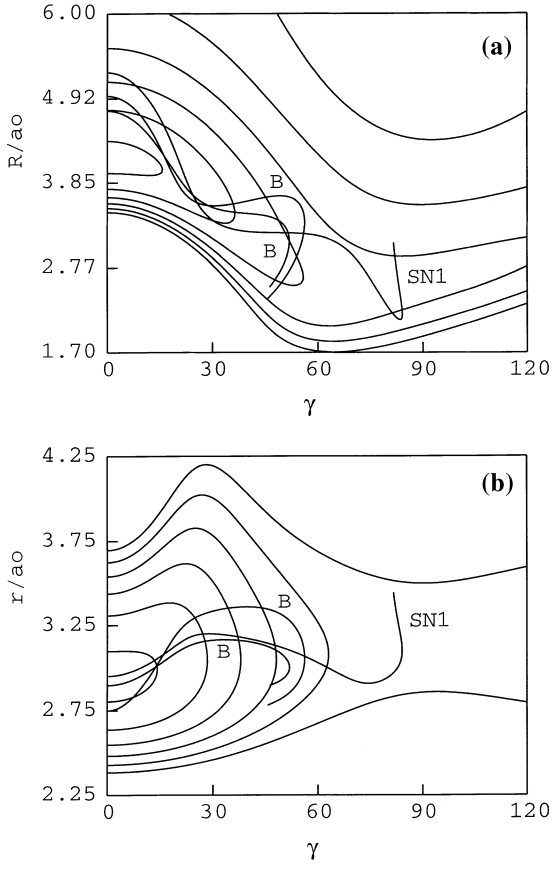

Fig. 3a, b Contour plots of the HCP potential energy surface **a** as a function of R and γ for fixed value of r and **b** as function of r and γ for fixed value of R. Energy normalization is such that $H + CP(r_e)$ corresponds to $E = 0$. The highest contour is for $E = 0$ and the spacing is $\Delta E = 1$ eV. Also shown are projections of selected classical POs: $[B]$, $E = -2.6217276$ and -1.6194926 eV; $[SN1]$, $E = -1.5284771$ eV

Contrary to the $[B]$ orbits, the SN PO shows a significant extension in the angular coordinate, well beyond 80°. This is the characteristic behavior of the $[SN]$ POs found for HCP. However, unlike HCP, the $[SN]$ POs for DCP are like the $[B]$-type orbits limited in their angular extension, at least in this energy regime. The $[SN]$ orbits for HCP extend much further into the CP–H hemisphere, even for considerably lower energies. This is a remarkable difference between HCP and DCP.

Apart from the shapes of the POS and their variation with energy, another piece of information which can be extracted is their stability, i.e., the behavior of trajectories in the vicinity of the POs. The stability is reflected by the eigenvalues of the monodromy matrix [20]. The $[B]$ family remains stable from the bottom of the potential well up to -3.15 eV where it turns to single unstable, i.e., one of the perpendicular directions of the PO becomes unstable with the neighboring trajectories deviating exponentially. The eigenvalue of the monodromy matrix, which corresponds to the unstable direction, reaches a maximum value of 57.51 at -1.11 eV.

The $[R]$ family shows an early period-doubling bifurcation at -4.645 eV giving rise to the family which is denoted as $[R1A]$ in the bifurcation diagram (Fig. 1). The $[R]$ family remains single unstable up to -3.58 eV where it becomes stable again and then remains stable for the whole energy interval studied. The bifurcating family $[R1A]$ is born stable and remains stable up to -1.7 eV where it becomes single unstable with a positive eigenvalue of the monodromy matrix equal to 2.67 at -1 eV of total energy. The $[r]$ family turns to single unstable at -3.87 eV and becomes double unstable at -1.95 eV. However, both positive eigenvalues of the monodromy matrix do not exceed values of 2.1 up to an energy of -1 eV. In other words, the $[r]$ family can be considered to be stable over a very large energy interval and the corresponding quantum states will show this.

The first SN bifurcation which we located is at -1.971 eV and it is single unstable with an eigenvalue of 60.6. This energy is only 0.08 eV below the energy of the saddle point of the PES. The POs of this type are symmetric with respect to the $\gamma = 0$ axis. The two branches differ in the second pair of their eigenvalues of the monodromy matrix with the $[SN1A]$ POs being single unstable and the $[SN1B]$ ones being double unstable. The period at the SN bifurcation is 135.4 fs. The $[SN1B]$ manifold turns into single unstable at -1.927 eV and it remains single unstable above -1 eV. The $[SN1A]$ orbits stay single unstable up to -1.416 eV with a huge positive eigenvalue of 27234. Beyond this energy they becomes double unstable. The eigenvalue in the new unstable direction is small, 1.75 at -1 eV, whereas the eigenvalue of the first unstable direction reaches the value of 68473 at -1 eV.

The above details for POs reveal the following dynamical picture for DCP. At some energy, the principal families turn from stable to single unstable but with small instability parameters. An early bifurcation appears in the $[R]$ family and this contrasts with what we found for HCP in which an early bifurcation in the $[r]$ family at -4.872 eV gives rise to the 1:2 resonance between the r and γ modes. For DCP, the $[R1A]$ bifurcation creates a 1:2 resonance between the R and r degrees of freedom. In the following we shall see that this resonance is also observed in the quantum mechanical wave functions.

Following the POs to very high energies confirms that the bending motion remains confined to small angles (less than 60°), as in the case of HCP (less than 40°). Extended angular motion is found only with the appearance of the SN bifurcation, just as in the case of HCP. However, in contrast to HCP this SN bifurcation comes to existence at a rather high energy (-1.971 eV) and, moreover, the corresponding POs are also restricted as far as the angular coordinate is concerned. We have not searched for other SN bifurcations at higher energies, which are expected to show bending motions with amplitudes larger than 90°. It turns out that for DCP there are effectively higher dynamical barriers preventing isomerization from D–CP to CP–D than in HCP. In what follows it will be shown that the overall behaviour of the quantum wave functions can be understood, at least qualitatively, in view of the PO analysis.

3.2.2 The quantum mechanical view

Several hundred vibrational levels and eigenfunctions have been computed for the rotationless DCP. In order to provide some idea about the energy range covered, we note that the 1000th state has an energy of -2.2412 eV in our calculation. Although we have visually examined a few hundred wave functions, only the first one hundred states plus some especially selected ones have been thoroughly assigned. The main purpose of this paper is to demonstrate the gross differences with HCP. The level structure and the assignments for the lower energy regime are presented in Fig. 4. In what follows, v_1, v_2, and v_3 denote the number of quanta in the D–CP stretching mode associated with R, the bending mode associated with γ, and the CP stretching mode related to motion in r, respectively. In most cases they indicate the number of nodes along the "backbone" of the respective wave function;[1,2] as will become apparent below, for some states a different assignment would be more meaningful.

The PO analysis has shown (see, for example, the periods in Fig. 1b) that the bending mode is quite uncoupled from the two stretching modes. (When comparing the periods of the three principal families in Fig. 1b one must take into consideration that the period of the $[B]$-type orbits corresponds to one bending quantum, whereas in the quantum mechanical calculations the energy gap between two bending levels corresponds to two quanta.) As a consequence, the pure bending states $(0, v_2, 0)$ remain unperturbed up to high energies. Plots of selected pure bending wave functions are shown in Fig. 5, the energy of the (0,16,0) level is -3.1428 eV. The wave functions behave as expected; however, it must be underlined that, in full accordance with the POs, they are restricted to an angular interval γ smaller than 60° or so and that increasing the energy does not force them to extend to larger angles. Note that 60° is exactly the angular regime where the minimum energy path in the (R, γ) plane changes direction (see Fig. 3a). It is not surprising that such a drastic feature of the potential might lead to some dynamical hindrance.

Because of the robustness of the bending states, it is meaningful to sort the quantum levels according to fixed quantum number v_2 as is done in Fig. 4. For HCP, it was more reasonable to arrange the energies according to v_1, the quantum number associated with the H–CP stretching mode, i.e., the mode that in HCP is weakly coupled to the other two. The 1:2 Fermi resonance found in the classical calculations also determines the quantum

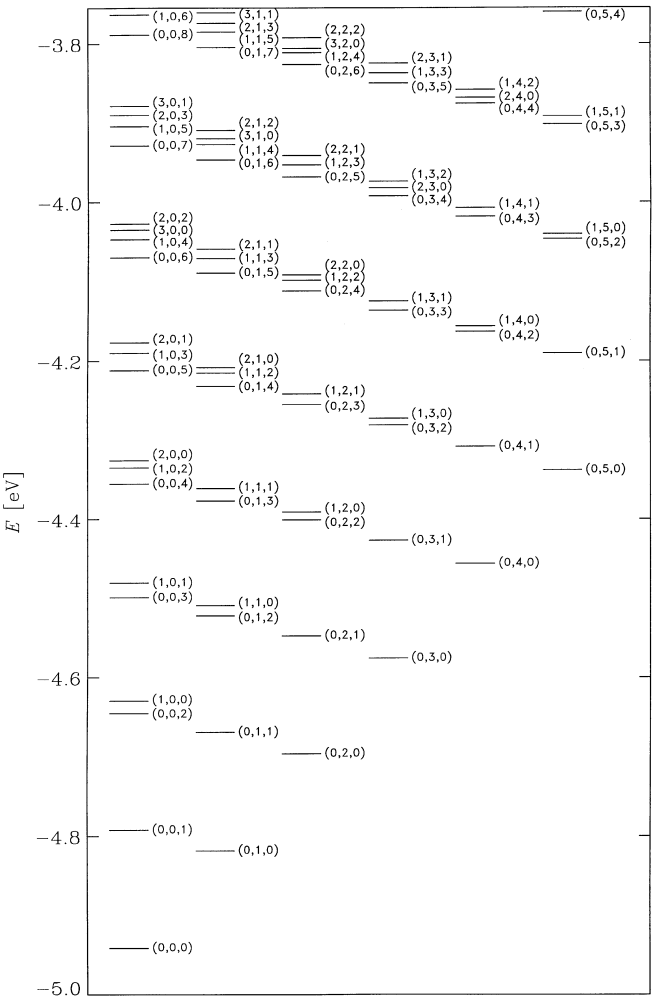

Fig. 4. Quantum mechanical energy level diagram. v_1, v_2, and v_3 denote the quantum numbers in the D–CP, the bending, and the C–P modes, respectively

mechanical level structure [13, 14]. Since two quanta in the CP stretch mode are roughly equal to one quantum in the D–CP stretching mode, the energy levels, for fixed value of v_2, show a clearly defined polyad structure with a "polyad quantum number" $P = 2v_1 + v_3$. The number of levels in each block is $P/2 + 1$ for even P and $P/2 + 1/2$ otherwise.

The pure $(0, 0, v_3)$ levels are the lowest ones in each polyad, with the gap to the next higher level slowly increasing with P. The corresponding wave functions have a very simple nodal behavior which qualitatively does not change up to high overtones. This robustness is in line with the stability of the corresponding $[r]$-type POs as discussed above. Examples are shown in the left-hand panel of Fig. 6. The wave function backbones are basically aligned along the minimum energy path of the potential and along the corresponding POs (compare with Fig. 2).

The situation is different for pure D–CP stretching states $(v_1, 0, 0)$. For the lowest polyads, the (1,0,0) and (2,0,0) levels are the highest ones within their respective polyads and the corresponding wave functions look as expected, i.e., they are aligned more or less perpendicu-

[1] In agreement with our previous work on HCP, the assignment of the bending overtones is given by the number of nodes of the wave functions in the angle interval from $\gamma = 0$ to 180° rather than by the traditional spectroscopic manner which doubles this bending quantum number. Thus, in order to compare with other assignments v_2 must be doubled

[2] All the wave function plots shown in this article have been obtained from a 3D plotting routine, which allows the rotation of objects that depend on three variables. In all cases we show one particular contour $\epsilon(R, r, \gamma) = \sin\gamma|\Psi(R, r, \gamma)|^2$. The plots are viewed either along the r axis (Fig. 5, left-hand panel), along the R axis (Fig. 5, right-hand panel), or along the γ axis (Figs. 6, 7)

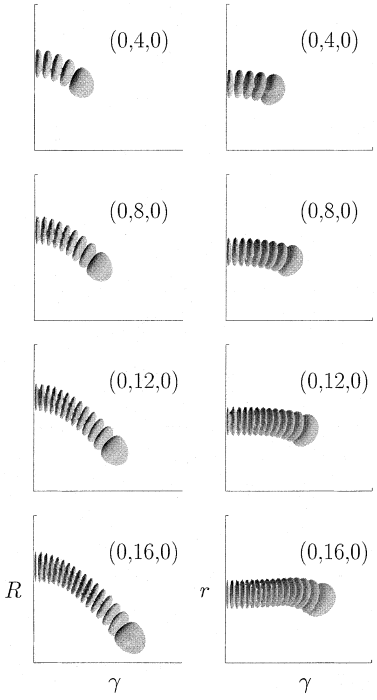

Fig. 5. Wave functions of selected bending overtones. The axes range from $R = 2.5a_0$ to $5.5a_0$, from $r = 2.2a_0$ to $4.0a_0$, and from $\gamma = 0$ to 70°

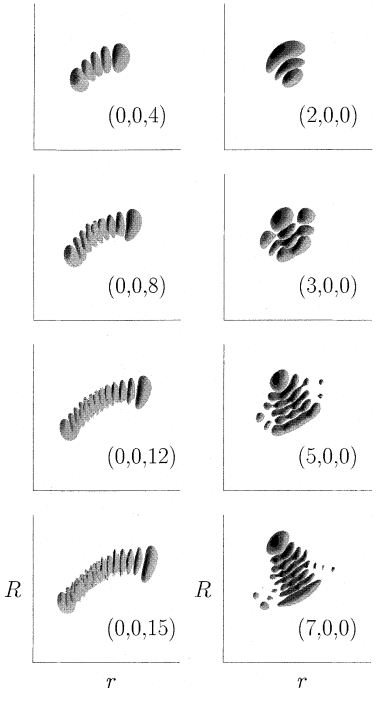

Fig. 6. Wave functions of selected C–P stretching (*left-hand panel*) and D–CP stretching (*right-hand panel*) overtones. The axes range from $R = 2.5a_0$ to $5.5a_0$ and from $r = 2.2a_0$ to $4.0a_0$

lar to the $(0, 0, v_3)$ wave functions, along the $[R]$-type POs, having one and two nodes, respectively (right-hand panel of Fig. 6). However, because of anharmonicity in the R coordinate (see, for example, the periods in Fig. 1b), the higher levels, (3,0,0) etc., move downwards within a particular polyad and are no longer the highest state. As a consequence, their energy separation from the other members of the polyad becomes smaller with the result that mixing with the one or the other neighbor becomes substantial. For example, state (3,0,0) has some large contribution from state (2,0,2) and likewise (4,0,0) has a large admixture of another nearby state. This behavior is in full accord with the observation made in the PO analysis, that the $[R]$ POs are unstable between the $[R]/[R1A]$ bifurcation and -3.58 eV. At higher energies the $[R]$-type orbits become stable again and the quantum wave functions show the same trend, namely the states $[v_1 \geq (5, 0, 0)]$ become more clearly recognizable again. The reason is probably that, due to anharmonicity, the pure $(v_1, 0, 0)$ states shift so much down to the lower end of the polyad that finally the coupling with the other states is negligibly small.

Up to now we have discussed only the pure overtone states $(v_1, 0, 0)$, $(0, v_2, 0)$, and $(0, 0, v_3)$. There are, of course, also clearly defined combination states: (1,0,1), (1,2,1), or (0,1,5), for example. Some of these combination states are strongly mixed with other states so a clear-cut assignment is not possible in terms of the nodal structure of the underlying wave functions. Not surprisingly, mixing becomes stronger with increasing energy. The first unassigned levels start at about no. 90 or so, at an energy only 1.1 eV above the zero-point level, that is, much earlier than in HCP.

The classical analysis also predicted some additional types of POs, those which bifurcate from the ones of the $[R]$ family and which somehow represent a mixture of R- and r-type motion (see Fig. 2). The question is then whether there are quantum states whose wave functions have a similar behavior? The answer is positive! They emanate from the $(v_1, 0, 1)$ and $(v_1, 0, 2)$ states. Examples are depicted in Fig. 7 as functions of R and r. They basically consist of two branches which are joined at the inner side of the potential well. With increasing excita-

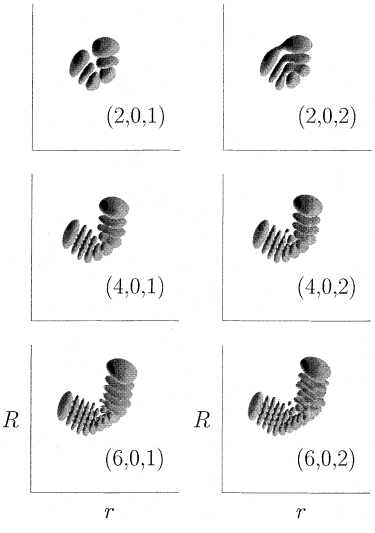

Fig. 7. Wave functions of selected $R1A$ states. The axes range from $R = 2.5a_0$ to $5.5a_0$ and from $r = 2.2a_0$ to $4.0a_0$

tion the gap between these two branches at the outer side of the well, toward the D + CP dissociation channel, opens considerably. The coincidence between these wave functions and the [*R*1*A*] POs in Fig. 2, which actually belong to a very high energy, is obvious – even without overlaying wave function and corresponding PO. These wave functions represent a new family of states, a manifold which is correctly predicted by the PO analysis. Actually, a better nomenclature would be $(P, v_2)_{R1A}$, where P counts the number of nodes along the backbone, v_2 is the bending quantum number, and the index *R*1*A* is a reminder that these states are actually born at the $R/R1A$ bifurcation. For example, (4,0,1) and (4,0,2), which belong to polyads 9 and 10, have 9 and 10 nodes along the backbone, respectively.

Finally, there is the question whether [*SN*]-type states, which represent large-amplitude motion of D around the CP core, exist in the way they were predicted for HCP. Classical mechanics predicts them to come into existence at energies much higher than for HCP. Our present quantum variational calculations are not accurate at such high energies and, therefore, we cannot verify their existence without doubt. Nevertheless, we searched for them up to an energy of -2.8 eV but did not find any evidence that similar states exist for DCP. This conclusion is also in full agreement with the PO analysis.

4 Conclusions

The vibrational dynamics of HCP and DCP are remarkably different. This is demonstrated by an analysis of the classical phase space as well as the quantum mechanical energy spectrum and wave functions. While in HCP a 1:2 resonance between the CP stretch and the bending modes largely determines the spectrum, in DCP it is a 1:2 resonance between the two stretches that leaves its unique hallmark. The latter leads to a special manifold of states, which we termed *R*1*A* states; they combine both motion in the D–CP stretch and the C–P stretch bond. SN states, which are characteristic for HCP, have not been found for DCP, at least not in the energy range considered in this work. The classical PO analysis predicts them to occur at energies significantly higher than for HCP.

The present study once more underlines the convincing relationship between POs, which manifest the structure of classical phase space, and the quantum mechanical spectrum. Without POs and their structural change with energy, the interpretation of the quantum mechanical results would be much more difficult.

Acknowledgements. S.C.F is grateful for the hospitality of the Max-Planck-Institut für Strömungsforschung where part of the classical analysis was accomplished. Financial support was obtained through the Sonderforschungsbereich 357 'Molekulare Mechanismen Unimolekularer Reaktionen'.

References

1. Keller H-M, Flöthmann H, Dobbyn AJ, Schinke R, Werner H-J, Bauer C, Rosmus P (1996) J Chem Phys 105: 4983
2. Keller H-M, Schröder T, Stumpf M, Stöck C, Temps F, Schinke R, Werner H-J, Bauer C, Rosmus P (1997) J Chem Phys 106: 5359
3. Mordaunt HD, Flöthmann H, Stumpf M, Keller H-M, Beck C, Schinke R, Yamashita K (1997) J Chem Phys 107: 6603
4. Farantos SC, Keller H-M, Schinke R, Yamashita K, Morokuma K (1996) J Chem Phys 104: 10055
5. Beck C, Keller H-M, Grebenshchikov SY, Schinke R, Farantos SC, Yamashita K, Morokuma K (1997) J Chem Phys 107: 9818
6. Lehmann KK, Ross SC, Lohr LL (1985) J Chem Phys 82: 4460
7. Chen Y-T, Watt DM, Field RW, Lehmann KK (1990) J Chem Phys 93: 2149
8. Mason MA, Lehmann KK (1993) J Chem Phys 98: 5184
9. Johns JWC, Shurvell HF, Tyler JK (1969) Can J Phys 47: 893
10. Cabaña A, Doucet Y, Garneau J-M, Pépin C, Puget P (1982) J Mol Spectrosc 96: 342
11. Ishikawa H, Chen Y-T, Ohshima Y, Rajaram B, Wang J, Field RW (1996) J Chem Phys 105: 7383
12. Ishikawa H, Nagao C, Mikami N, Field RW (1997) J Chem Phys 106: 2980
13. Botschwina P, Sebald P (1983) J Mol Spectrosc 100: 1
14. Puzzarini C, Tarroni R, Palmieri P, Demaison J, Senent ML (1996) J Chem Phys 105: 3132
15. Kellman ME (1995) In: Dai H-L, Field RW (eds) Molecular dynamics and spectroscopy by stimulated emission pumping. World Scientific, Singapore, p 943
16 Kellman ME (1995) Annu Rev Phys Chem 46: 395
17. Gutzwiller MC (1990) Chaos in classical and quantum mechanics, vol 1. Springer, Berlin Heidelberg Newyork
18. Llorente JMG, Pollak E (1992) Annu Rev Phys Chem 43: 91
19. Taylor HS (1995) In: Dai H-L, Field RW (eds) Molecular dynamics and spectroscopy by stimulated emission pumping. World Scientific, Singapore, p 891
20. Farantos SC (1996) Int Rev Phys Chem 15: 345
21. Farantos SC (1998) Comput Phys Commum 108: 240
22. Dobbyn AJ, Stumpf M, Keller H, Schinke R (1995) J Chem Phys 103: 9947